Enhanced Treatment Efficiency of Holmium:YAG Laser Lithotripsy by Using PEDOT:PSS Nanofluid

Qingsong Fan[1ǂ], Junqin Chen[2ǂ], Faisal Anees[2], Judith Dominguez[2], Ting-Hsuan Chen[1], Christine Payne[2], Pei Zhong[2*], Po-Chun Hsu[1*]

1: Pritzker School of Molecular Engineering, University of Chicago

2: Thomas Lord Department of Mechanical Engineering and Materials Science, Duke University

ǂ: These authors contribute equally

Abstract

Holmium: yttrium-aluminum-garnet (Ho:YAG) laser lithotripsy has been considered the gold standard for treating urinary stones, a disease with increasing prevalence in the US in recent years. While various efforts have been made to enhance the stone ablation efficiency of Ho:YAG laser, these have primarily focused on adjusting laser source settings such as pulse energy and frequency. In this study, we introduced a novel strategy to improve the ablation efficiency of the Ho:YAG laser by incorporating nanoparticles into the fluid surrounding the stone with strong near-infrared light absorption. Experimental results of stone damage revealed an 82% increase in photothermal ablation efficiency when using a "dusting" mode of laser lithotripsy in 0.03 wt.% PEDOT:PSS solution in direct contact. The enhanced NIR absorbance of the fluid was found to promote vapor tunnel formation, facilitating increased laser energy transmission to the stone surface, and to enhance stone absorbance due to trapped fluid inside, leading to greater laser energy absorption for photothermal ablation. Furthermore, cytotoxicity tests on PEDOT:PSS solution demonstrated minimal toxicity when carefully controlling concentration and application duration. This modification of fluid absorbance for efficiency improvement presents a versatile approach compatible with previously reported laser setting modulation methods, showcasing significant potential for enhancing Ho:YAG laser lithotripsy.

Keywords: Kidney stone disease, laser lithotripsy, Ho:YAG laser, ablation efficiency, NIR absorber

Introduction

Urinary stone disease (USD) is a benign yet severely painful genitourinary condition affecting nearly 1 in 11 Americans. In 2000, the annual health expenditure for USD in the US exceeded $2 billion, and this figure continues to rise rapidly today[1–3]. Minerals such as calcium oxalate, calcium phosphate, and uric acid gradually crystallize and form large stones when they cannot be completely expelled from the urinary system. When these stones grow to a size capable of obstructing urine flow, they cause intense pain along with additional symptoms like frequent urination, difficulty urinating, and blood in the urine. Fortunately, various modalities have been developed to remove urinary stones, including extracorporeal shock wave lithotripsy (ESWL), ureteroscopy (URS), percutaneous surgery, and open stone surgery[4].

Despite the advantages of non-invasiveness and anesthesia-free treatment, numerous studies have reported that ESWL exhibits lower efficacy in managing large (> 1 cm) or hard stones, resulting in reduced clearance and stone-free rates[5–7]. Intracorporeal lithotripsy constitutes a fundamental aspect of both percutaneous surgery and ureteroscopy. Various intracorporeal lithotripters have been utilized to fragment urinary tract stones, ranging from ultrasonic[8], electrohydraulic[9], and pneumatic devices[10] to urinary electrokinetic devices[11] and lasers[12]. Since its initial implementation in the early 1990s[13], the past three decades have seen significant advancements in laser lithotripsy equipment, particularly those

utilizing the holmium: yttrium-aluminum-garnet (Ho:YAG) laser[14,15]. When compared to alternative lithotripters (such as ultrasonic, electrohydraulic, and pneumatic devices) and laser sources (such as ruby, pulsed-dye, continuous-wave Nd:YAG, and Q-switched Nd:YAG lasers), Ho:YAG laser lithotripsy (LL) offers numerous advantages. These include its efficacy in fragmenting all types of stones[16,17], minimal retropulsion[18], and compatibility with low-cost flexible optical fibers. More importantly, large series have shown that Ho:YAG laser lithotripsy is safe in children[19–21], in all stages of pregnancy[22] and in patients with bleeding disorders[23,24]. Consequently, it has emerged as the gold standard procedure in laser lithotripsy[25].

Over the centuries, researchers have endeavored to enhance the ablation efficiency of Ho:YAG LL. The majority of these efforts have focused on manipulating the laser output profile, including pulse energy, pulse duration, and frequency[26–30]. Despite documented improvements in efficiency resulting from these techniques in the literature, very few researchers have explored modifications to the fluid surrounding the stones. Recently, Giglio et al.[31] and Saeed et al.[32] investigated the impact of adding surfactants to water on the behavior of laser-induced vapor bubbles. Although they observed elongated bubble lengths and lifetimes attributed to reduced surface tension of the fluid, the ablation efficiency of the stones was not explored.

Inspired by the recently developed thulium fiber laser, which has been shown to be two-four times more ablative than the widely used Ho:YAG laser due to its wavelength more closely matching the absorption peak of water[33,34], we propose that enhancing the absorption of laser energy through the addition of nanoparticles capable of absorbing infrared light could also enhance the ablation efficiency of Ho:YAG laser lithotripsy. In this study, we showcased the enhanced ablation efficiency of Ho:YAG laser lithotripsy through the introduction of poly(3,4-ethylenedioxythiophene) polystyrene sulfonate (PEDOT:PSS) nanoparticles, a well-established polymeric material known for its absorption peak in the near-infrared spectrum, into the fluid. Laser lithotripsy conducted in a 0.03 wt.% PEDOT:PSS solution demonstrated a minimum of 80% improvement in photothermal ablation compared to procedures conducted in water across all investigated standoff distances (0-1 mm). Additionally, we delved into the mechanism behind this enhanced ablation efficiency by examining bubble dynamics and stone reflectance after soaking. Our findings suggest that both the accelerated expansion of the vapor bubble in the PEDOT:PSS solution and the heightened absorption of laser energy by the fluid trapped within the stones contribute to the observed enhancement in photothermal ablation.

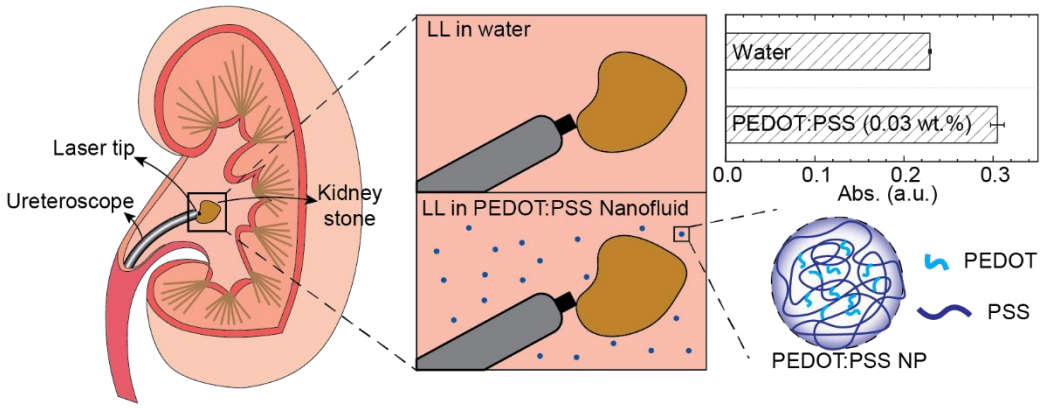

Scheme 1. Schematic illustration of the application of laser lithotripsy in kidney stone removal. Traditional laser lithotripsy is conducted in saline (water) which has a limited absorption at 2120 nm. By introducing PEDOT:PSS nanoparticles in the fluid, which has an enhanced absorption at 2120 nm, the stone damage efficiency of laser lithotripsy can be improved.

Results and Discussion

Optical properties of PEDOT:PSS nanofluid

PEDOT:PSS stands out as one of the most promising conductive polymers, finding widespread applications in flexible electronics[35–37], solar cells[38,39], IR sensors[40], and more. Its appeal lies in its tunable electrical conductivity, relative transparency to visible light, excellent thermal stability, and biocompatibility[41]. Moreover, PEDOT:PSS nanoparticles (NPs) are conveniently synthesized through colloidal routes[42], facilitating large-scale production at a relatively low cost. PEDOT:PSS is also known for its pronounced absorption of near-infrared (NIR) light. As depicted in **Figure 1a**, the addition of PEDOT:PSS NPs to water leads to a gradual increase in fluid absorbance within the NIR range. Of particular interest is the absorbance of fluids at 2120 nm, the operational wavelength of the Ho:YAG laser utilized in laser lithotripsy. Through plotting absorbance at 2120 nm against the concentrations of PEDOT:PSS solutions, a linear correlation emerges between these parameters. Consequently, as the concentration of the PEDOT:PSS solution rises, the penetration depth of light at 2120 nm diminishes. For instance, the penetration depth decreases from 379.6 ± 2.2 μm for pure water to 285.3 ± 6.9 μm for the PEDOT:PSS solution with a concentration of 0.03 wt.%, corresponding to a ~25% reduction.

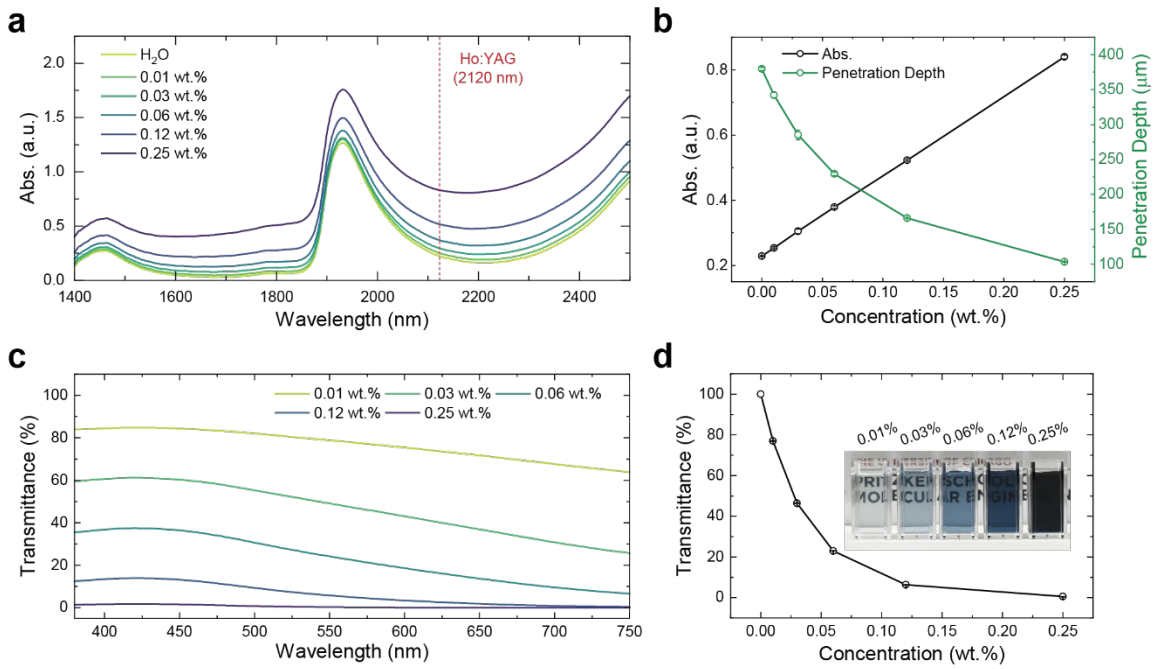

Figure 1. Optical properties of PEDOT:PSS aqueous solution**.** (a) Absorbance spectra of water and PEDOT:PSS solutions of different concentrations within the NIR range (path length of measurements: 0.2 mm). (b) The absorbance and derived penetration depth values at the wavelength of 2120 nm of PEDOT:PSS solutions. (c) Transmittance of PEDOT:PSS solutions in visible spectrum (path length of measurements: 5 mm). (d) The calculated average transmittance in visible of PEDOT:PSS solutions over a wavelength range of 380-750 nm (inset: a digital photo of PEDOT:PSS solutions at different concentrations in cuvettes with a 5 mm path length).

Although the addition of PEDOT:PSS NPs in water can significantly enhance the NIR absorption of the fluid, the non-negligible absorption of PEDOT:PSS of visible light due to the π- π* transition[43] makes the solution appear as a dark blue fluid, especially at high concentrations (**Figure 1d**, inset). This strong visible absorption contradicts with the stringent requirement of a clear field of view for the surgeon during the laser lithotripsy. To find out the optimal concentration of PEDOT:PSS solution for laser lithotripsy by considering both NIR absorbance enhancement and visibility, we measured the transmittance of the above solutions within visible regime (**Figure 1c**). The path length was chosen to be 5 mm to mimic the typical distance between the ureteroscope and the kidney stone during laser lithotripsy. The average transmittance of the solutions within the visible was also calculated, and as expected, it decreases with increasing PEDOT:PSS concentration. Upon inspection of the field of view under the ureteroscope, we observed that the kidney stone remains clearly visible in the PEDOT:PSS solution when the concentration does not exceed 0.03 wt.% (**Figure S1**), indicating that an average transmittance of approximately 50% or higher at a path length of 5 mm must be maintained when employing a solution as the fluid for laser lithotripsy.

Stone damage assessment

We then assessed the stone damage efficiency of three different fluids by conducting laser lithotripsy using the "Dusting" mode (low pulse energy, high frequency) in a cuvette containing an artificial BegoStone immersed in the fluid. The cuvette's geometry is depicted in **Figure 2a**, and a ureteroscope-integrated laser fiber was placed atop the stone at various standoff distances (SDs) (e.g., 0, 0.5, and 1.0 mm). Ideally, maximizing photothermal ablation entails direct contact between the laser fiber tip and the stone surface. However, maintaining such contact is unrealistic in clinical practices due to retropulsion. Therefore, we investigated enhancement levels at various SDs. **Figure 2b** depicts typical crater images on BegoStone phantoms produced in different PEDOT:PSS solutions at SD = 0 – 1 mm, with corresponding dimensional measurements summarized in **Figure 2d**. First, as the concentrations of PEDOT increased, the size of damage craters expanded across all SDs. Faint blue tints were consistently observed inside the craters when PEDOT:PSS solutions were employed. We attribute such coloration to the adherence of PEDOT:PSS NPs to the stone surface due to the local high temperatures induced by complex laser-stone interactions. Furthermore, compared to the regular and round craters produced at SD = 0 and 1 mm, the profiles of the craters produced at SD = 0.5 mm exhibited irregularities in all three fluids, suggesting the critical contributions of bubble collapse in stone damage[44,45].

Quantitatively, at each SD, we observed a significant increase in crater volume with the addition of PEDOT:PSS to the fluid. For instance, at SD = 0 mm, i.e., as the photothermal ablation dominates, the stone treatment in 0.01 wt.% and 0.03 wt.% PEDOT:PSS solutions resulted in crater volume increases of 38% (0.0848 ± 0.0182 mm^3) and 114% (0.1313 ± 0.0287 mm^3), respectively, when compared to those produced in pure water (0.0614 ± 0.0092 mm^3) under the same conditions. This enhancement in ablation efficiency was ascribed to the increase of both maximum depth and profile area. Similarly, as SD increased to 1 mm, although the ablation efficiency dropped dramatically in all three fluids due to the absorption of laser energy by the fluid, laser treatment in 0.03 wt.% PEDOT:PSS solution exhibited a 736% enhancement in crater volume compared to water (0.01554 ± 0.00652 mm^3 vs. 0.00188 ± 0.00173 mm^3), suggesting the unique advantages of using PEDOT:PSS solutions for expanding the efficient fiber-to-stone working distance during LL. More interestingly, for all three fluids tested, the greatest stone damage was produced at SD = 0.5 mm with an enhancement of 19% in 0.01 wt.% and 38% in 0.03 wt.% PEDOT:PSS solutions, suggesting that there may exist an optimal combinations of SDs and PEDOT:PSS concentrations for maximizing the treatment efficiency of LL.

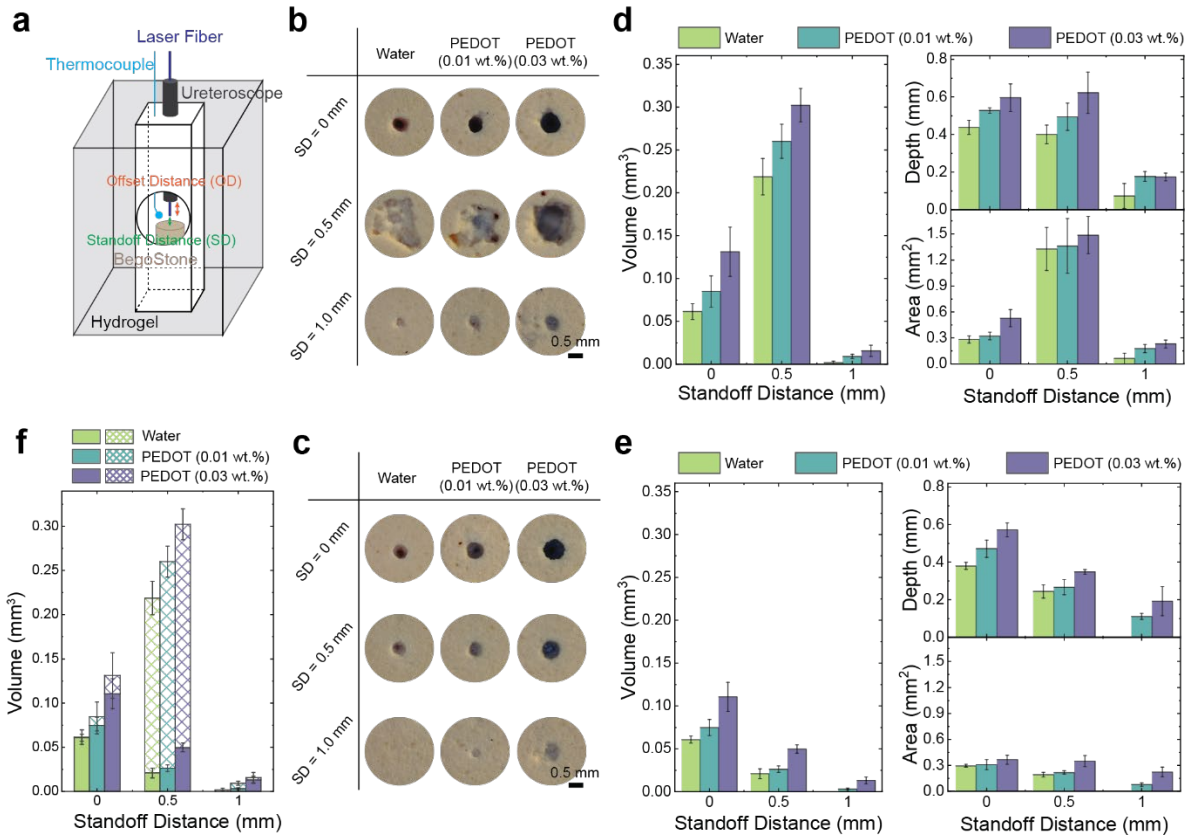

Figure 2. Stone damage assessment. (a) Schematic illustration of experimental setup. (b, c) Digital photos of craters produced on top of the Bego stones produced with an OD of 3 mm (b) and 0.25 mm (c). (d, e) Dimensional measurements of craters by OCT for produced with an OD of 3 mm (d) and 0.25 mm (e). (The values and error bars are the average results and standard deviations of 5 independent experiments under each condition). (f) The contribution of thermal decomposition and cavitation to the crater's volume (thermal decomposition and cavitation induced ablation are represented by the solid and meshed bars, respectively).

To further differentiate the contributions of thermal ablation and cavitation in different PEDOT:PSS solutions, we conducted control experiments where all parameters remained constant, except for the distance between the laser tip and the ureteroscope (offset distance, OD). We compared the stone damage produced at a smaller OD (0.25 mm) to those produced at a larger OD (3 mm). The former scenario can distract the bubble collapse away from the stone surface as demonstrated in **Figure S2** and thus eliminate the cavitation damage[45]. The digital photos and dimensional measurements of the resultant craters are summarized in **Figures 2c** and **2e**. The craters produced at SD = 0 and 1 mm with a short OD closely resembled those in experiments with an OD of 3 mm (**Figure 2d**), indicating that cavitation may play a negligible role in stone damage at these two SDs. In contrast, the most notable difference emerged when SD was set to 0.5 mm: since the cavitation effect was eliminated, the obtained craters exhibited circular profiles similar to those produced at other SDs. Additionally, with the scope at OD = 0.25 mm, the volume of the craters decreased as the laser tip moved further away from the stone, consistent with the characteristics of stone damage caused by thermal ablation.

Combining the results from Figures 2d and 2e allows us to discern the contributions of thermal decomposition and cavitation to stone damage under various experimental conditions (**Figure 2f**). It is evident that the enhanced ablation efficiency primarily stems from improved photothermal ablation. At SD = 0 mm, compared to laser lithotripsy in water (0.0607 ± 0.0041 mm^3), photothermal ablation shows a 23% (0.0747 ± 0.0094 mm^3) and 82% (0.1106 ± 0.0167 mm^3) improvement in 0.01 wt.% and 0.03 wt.% PEDOT:PSS aqueous solutions, respectively. Similarly, at SD = 0.5 mm, the improvement in photothermal ablation is 25% (0.0262 ± 0.0037 mm^3) and 138% (0.0498 ± 0.0048 mm^3) compared to laser lithotripsy in water (0.0209 ± 0.0057 mm^3). **Figure 2f** also indicates a slight enhancement in cavitation when PEDOT:PSS NPs are added. Overall, the introduction of PEDOT:PSS NPs into the fluid significantly improves the ablation efficiency of Ho:YAG laser lithotripsy, primarily through enhanced photothermal ablation, at all SDs, demonstrating its great potential for urinary stone treatment.

Bubble dynamics

To elucidate the mechanism behind the enhanced photothermal ablation of stones, we examined the expansion of bubbles in different fluids using a high-speed camera (Phantom v7.3, Vision Research, Wayne, NJ) operating at 100,000 frames per second. **Figures 3a** and **3b** depict the initial frames of bubble generation and expansion during laser lithotripsy in three different fluids at SDs of 0.5 mm and 1 mm, respectively. To replicate the laser-fluid-stone interaction during LL, a glass slide was placed in front of the fiber at a certain distance. We measured the distance between the fiber tip and the bubble front in each frame and summarized the results in **Figure 3c** (see **Supplementary Material**). It is evident that the bubble in 0.03 wt.% PEDOT:PSS solution expanded the fastest at both SDs. Furthermore, we calculated the temporal transmittance of 2120 nm light by considering the absorption coefficients and distances in the fluid and vapor (**Figure S5**). By multiplying the temporal transmittance of 2120 nm light at different SDs with the output power of the laser (**Figure 3d**, top), we obtained the time-dependent transmitted powers at these SDs (**Figure 3d**, middle and bottom). Higher laser powers could be transmitted at the early stage of each pulse due to the faster establishment of the vapor tunnel in 0.03 wt.% PEDOT:PSS solution. The transmitted energy was then calculated by integrating the transmitted power over time. In **Figure 3e**, we assumed that the laser energy of each pulse could be transmitted with no loss (0.2 J) at the SD of 0 mm. Intuitively, less laser energy is transmitted as the SD increases, with the energy loss primarily caused by fluid absorption in between.

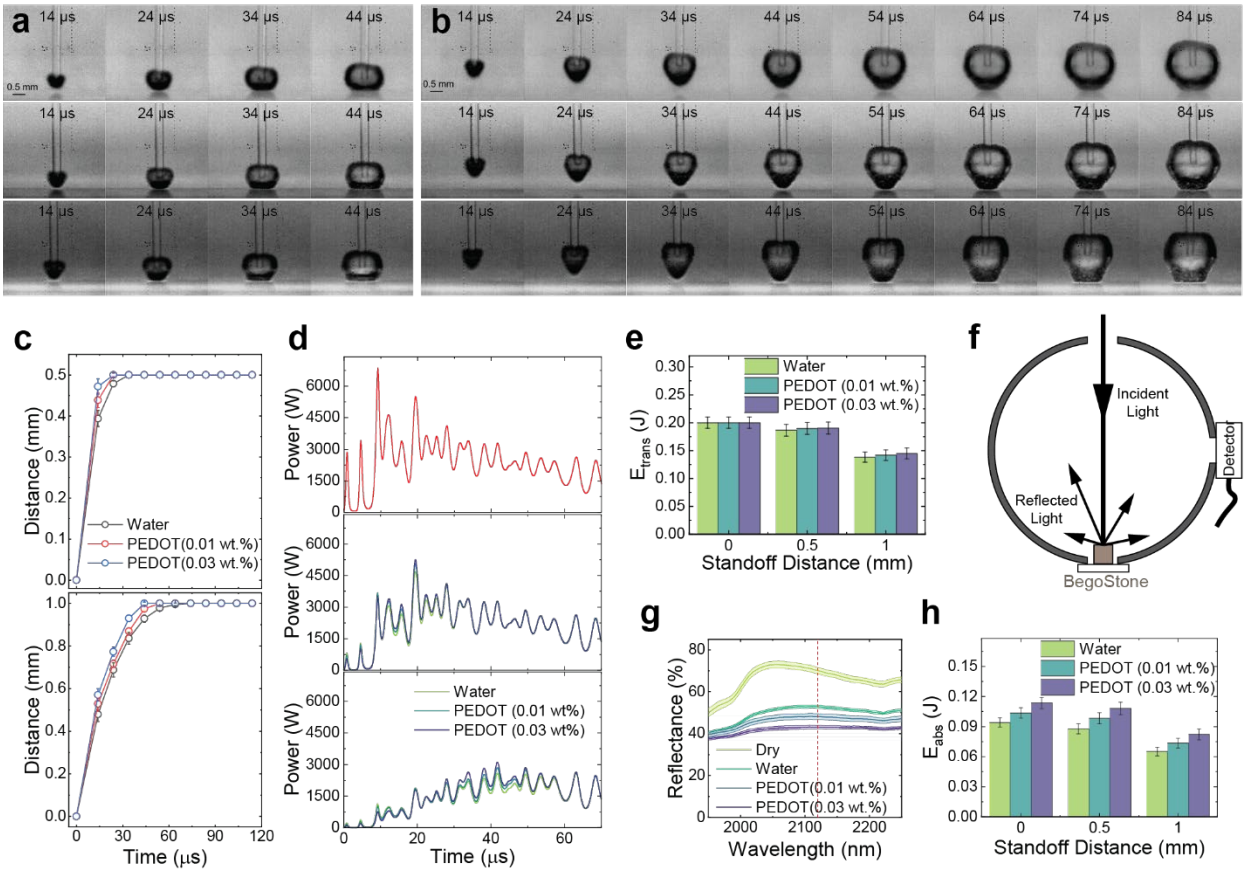

Figure 3. Bubble dynamics and calculated laser energies. (a, b) Snapshots of bubbles generation and expansion during one pulse of the laser lithotripsy in different fluids (from top to bottom: water, 0.01 wt.%, and 0.03 wt.% PEDOT:PSS solution) with a glass slide placed at a distance of 0.5 mm (a) and 1 mm (b) in front of the laser fiber. (c) Temporal change of the distance between fiber and bubble front in various fluids (top: SD = 0.5 mm, bottom: SD = 1 mm. Error bars are standard deviations of 45 measurements). (d) The output power of the 60th pulse of the Ho:YAG laser (top) and calculated transmitted powers in different fluids (middle: SD = 0.5 mm, bottom: SD = 1 mm). (e) Calculated average transmitted energy at different SDs (Error bars are standard deviations of 45 measurements). (f) Scheme of NIR reflectance measurement of the soaked stones using an integrating sphere. (g) Measured NIR reflectance of stones. (h) Calculated energy absorbed by the stones soaked with various fluids.

However, comparing the transmitted energies in PEDOT:PSS solutions to those in water at the same SD reveals a subtle increasing trend. For example, there was only a 4.8% increase in transmitted energy for 0.03 wt.% PEDOT:PSS compared to water (0.1449 ± 0.0098 J vs. 0.1383 ± 0.0092 J) at the SD of 1 mm. Similarly, this increase was only 2.1% at the SD of 0.5 mm (0.1903 ± 0.0109 J vs. 0.1864 ± 0.0106 J). This slight increase in transmitted energy cannot account for the significant improvement in ablation efficiency demonstrated in **Figure 2f**.

It is widely recognized that instead of a condensed, solid stone, BegoStone contains numerous submillimeter pores[46]. When the stone is immersed in fluid, the fluid diffuses into the stone and occupy the small pores. Additionally, when PEDOT:PSS solution is used as the fluid, PEDOT:PSS NPs may

attach to the stone surface. Thus, we suspect that both PEDOT:PSS NPs trapped in the pores and those attached to the stone's surface contribute to increased absorption of laser energy transmitted to the stone. To verify our hypothesis, we measured the NIR reflectance of BegoStones with various trapped fluids using a spectrometer equipped with an integrating sphere (**Figure 3f**), and the results are summarized in **Figure 3g** (see Methods). As anticipated, stone reflectance at 2120 nm decreased from 52.9% to 43.2% when water was replaced with 0.03 wt.% PEDOT solution. Finally, by considering both transmitted energy and BegoStone absorption when soaked with fluids, we derived the absorbed energy. **Figure 3h** illustrates a 20.6% (0.0942 ± 0.0046 J vs. 0.1136 ± 0.0056 J), 23.2% (0.0878 ± 0.0049 J vs. 0.1082 ± 0.0061 J), and 26.2% (0.0652 ± 0.0043 J vs. 0.0823 ± 0.0055 J) increase in absorbed energy in 0.03 wt.% PEDOT:PSS solution compared to water, at SDs of 0, 0.5, and 1 mm, respectively.

Aside from the increased absorbed laser energy accounting for the enhanced photothermal ablation, we believe that micro-explosions of the trapped PEDOT:PSS solution inside the stone also contribute to the improved overall ablation efficiency. However, experimental and theoretical verification related to this contribution are complex and will be investigated in future studies.

Similar faster bubble expansion behavior was also observed in experiments where surfactants were added to water to reduce its surface tension[31,32]. However, unlike surfactants, which have amphiphilic molecular structures, PEDOT:PSS NPs have a hydrophilic shell that enables their dispersity in water[41]. Therefore, when these NPs are dispersed in water, they remain inside the water instead of at the water-air interface, resulting in no change to the surface tension. To confirm this, we measured the surface tension of PEDOT:PSS solutions with various concentrations (**Figure S7**). The results showed that within the investigated concentration range, the surface tension of the fluid remained constant and close to that of water. This finding demonstrates that the faster expansion of vapor bubbles in PEDOT:PSS solution is solely due to its enhanced NIR absorbance, indicating a distinct mechanism from previous work.

Cytotoxicity

The toxicity of PEDOT:PSS NPs must be investigated before their application in clinical practice. Thus, we incubated Murine epithelial cells with PEDOT:PSS solutions of various concentrations (0.006 wt.% to 0.1 wt.%) for different durations (1 hour or 24 hours). The cell viabilities from all experiments are summarized in **Figure 4**. In the cytotoxicity test, only cells incubated in 0.05 wt.% and 0.1 wt.% PEDOT:PSS solutions exhibited a noticeable decrease in cell viability at both durations. Considering the moderate concentration (⩽ 0.03 wt.%) and the typical duration of laser lithotripsy treatment (~1 hours), the use of PEDOT:PSS solution in laser lithotripsy demonstrates very limited toxicity to human kidney tissues.

The temperature increase is another concern in clinical practice due to the potential thermal injury to kidney tissue[47,48]. According to recorded temperature changes during the stone damage experiment, there was an abrupt temperature rise when the laser was activated in all three fluids (water, 0.01 wt.%, and 0.03 wt.% PEDOT:PSS solutions, **Figure S8**). Although the temperature rise was higher in PEDOT:PSS solutions compared to water (water: 0.934 K, 0.01 wt.%: 1.134 K, 0.03 wt.%: 1.191 K), such a limited temperature increase could be easily compensated by using a slightly larger irrigation flow. Furthermore, the significant improvement in ablation efficiency demonstrated in this work using 0.03 wt.% PEDOT:PSS solution has great potential to shorten treatment duration. In this sense, utilizing PEDOT:PSS solution for laser lithotripsy may in turn reduce the risk of thermal injury.

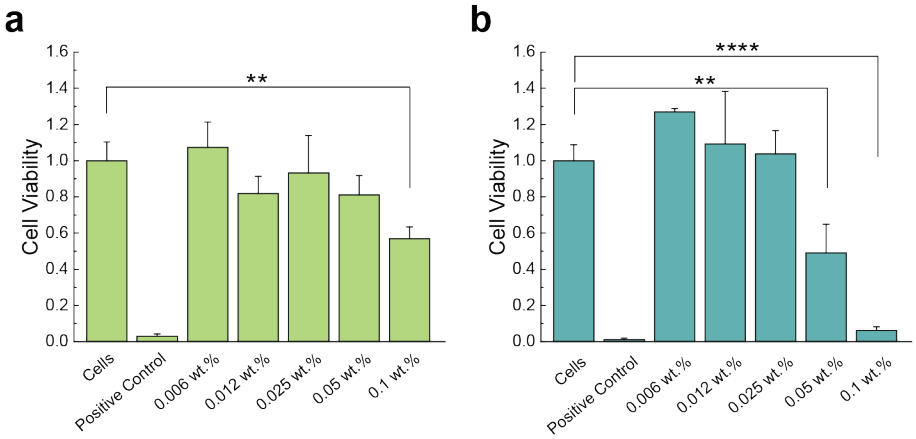

Figure 4. Viability of mIMCD-3 cells, measured with a MTT assay, after incubation with increasing concentrations of PEDOT:PSS. Exposure to triton X-100 (10% in PBS, 30 s) was used as a positive control to decrease cell viability. (a) 1 h incubation. (b) 24 h incubation. Significance was measured using 1-way ANOVA with Dunnett's multiple comparisons post hoc. **$p<0.01$, ****$p<0.0001$, ns – not significant not shown.

Conclusion

In this study, we presented a novel approach to enhance the ablation efficiency of Ho:YAG laser lithotripsy by incorporating PEDOT:PSS NPs into the fluid. At a concentration of 0.03 wt.%, PEDOT:PSS solution exhibited a 25% reduction in penetration depth of the Ho:YAG laser wavelength compared to water. Notably, when operated in direct contact mode, this solution demonstrated an 82% increase in photothermal ablation efficiency. Furthermore, this enhancement became more pronounced with increasing standoff distance, suggesting its ability to extend the laser's working distance.

The observed improvement in photothermal ablation was attributed to two factors: firstly, the rapid establishment of a vapor tunnel facilitated more laser energy transmitted to the stone surface; secondly, the enhanced laser energy absorption due to PEDOT:PSS NPs trapped within stone pores and adhered to the stone surface. Cell viability tests conducted over a typical treatment duration of 1 hour revealed minimal cytotoxicity associated with PEDOT:PSS solutions at this concentration. Additionally, the temperature rise resulting from enhanced fluid absorption had only a limited effect, which could be easily managed within controllable levels.

Overall, PEDOT:PSS solution has demonstrated significant potential for enhancing the efficiency of Ho:YAG laser lithotripsy in removing urinary stones. Our work distinguishes itself from previous studies by leveraging NIR absorber-induced efficiency improvements, marking a notable advancement in this field.

Materials and Methods

Aqueous Dispersion of PEDOT:PSS Conductive Polymer (Clevios PH 1000) was purchased from MSE Supplies and used without further purification. The solution has a concentration of 1.2 wt.% and the average particle size is 30 nm. The solution was diluted by DI water into various concentrations.

Near-IR absorption spectroscopy: The NIR absorbance spectra of solutions were measured using a UV-Vis-NIR spectrophotometer (Cary 5000, Agilent). During the measurement, the solution was filled in a cuvette with a path length of 0.2 mm (IR quartz, FireflySci, Inc.) and the scan range was set to be 1350 – 2500 nm (resolution: 1 nm and scan rate: 600 nm/min). The slit width was 1 nm. An empty cuvette was used as the background when collecting data.

Visible transmission spectroscopy: The visible spectra were measured on the UV-Vis-NIR spectrophotometer (Cary 5000, Agilent). The scan range was set to be 380 – 750 nm (resolution: 1 nm and scan rate: 600 nm/min). The slit width was 1 nm. A glass cuvette with a path length of 5 mm filled with water was used as the background when collecting data. The average transmittance of a solution in visible is calculated by:

$$\%T_{average} = \frac{\int_{380}^{750} \%T_{measured}\, d\lambda}{\int_{380}^{750} d\lambda}$$

NIR diffusive reflectance: The NIR diffusive reflectance of the BegoStone samples was measured using a UV-Vis-NIR spectrometer (Shimadzu UV3600 Plus) equipped with an integrating sphere. The scan range was set to be 1950 – 2250 nm (resolution: 1 nm and scan rate: medium). The slit width was 1 nm. A standard white plate coated with BaSO4 was used as the reference. 30 uL of the fluid is dropped on the top surface of the BegoStone and it quickly diffused into the stone within 30 s and no liquid can be observed on the stone surface. For each fluid, same measurement was repeat on seven different stones to account for the variation in stones. The average of seven measurements and standard deviation (colored shade) were plotted in Figure 3g. Since BegoStone is very thick (6 mm), we assume no light can transmit through, so stone absorption = 1 – reflectance.

Stone Damage Assessment: To evaluate the impact of PEDOT:PSS nanofluids on the stone damage efficiency of LL, we treated artificial BegoStone phantoms (6 x 6 mm pre-soaked cylinders; 5:2 powder to water ratio, BEGO USA, Lincoln, RI, USA) in a cuvette by using a clinical Ho:YAG laser lithotripter (H Solvo 35-watt laser, Dornier MedTech, Munich, Germany). Within the cuvette, a thick layer of transparent hydrogel (Gelatin #1; Humimic Medical, SC, USA) was applied to its inner walls to simulate the soft boundary of kidney tissue, leaving a 12*12*40 mm^3 cuboid space in the middle as depicted in Figure 2a. To further mimic a calyx environment of the kidney, a 3D-printed part with a spherical chamber of 5 mm in radius was fixed in the cuboid. The chamber was filled with 2 mL of PEDOT:PSS solutions at different concentrations (0 wt.%, 0.01 wt.%, and 0.03 wt.%) and the stone sample was positioned in its center. Additionally, a thermocouple was placed near the tissue boundary to record fluid temperature changes during LL. During the treatment, a flexible ureteroscope (Dornier AXISTM, with a 3.6 F working channel from Munich, Germany) with a 270 µm laser delivery fiber (Dornier SingleFlex 200, Munich, Germany) inserted through its working channel was placed perpendicularly to the stone surface. Laser pulses (60 pulses, n = 5) were delivered at an energy level of E_p = 0.2 J and a frequency of F = 20 Hz in dusting mode at various fiber tip-to-stone standoff distances (SDs; 0, 0.5, and 1.0 mm). The resultant damage craters were then scanned by optical coherence tomography (OCT) to extract crater volumes, depths and profile areas.[44]

Cell Culture: A murine epithelial cell line (mIMCD-3, ATCC, Manassas, VA) was used for all experiments. Cells were cultured in Dulbecco's Modified Eagle Medium/Hams F-12 (DMEM/F-12; pH 7.4, #11320033, Thermo Fisher), supplemented with 10 % fetal bovine serum (FBS, #10437028, Thermo Fisher, Waltham, MA). Cells were grown at 5% CO_2 at 37 °C and passaged upon reaching 80% confluency with a maximum passage number of 20.

MTT Assay: MIMCD-3 cells were seeded onto sterile 24-well plates (#3524, Corning Inc, Corning NY) at a density of 150,000 cells per well. The cells were cultured overnight and incubated with PEDOT:PSS (0.006 wt.%-0.1 wt.%) for 1 h or 24 h. Control cells were incubated in DMEM/F-12 media for the duration of the treatment. Incubation with Triton X-100 (10% in Dulbecco's Phosphate Buffered Saline (PBS), 30 s exposure; X100-100ML, Millipore Sigma, Burlington, MA) was used to damage cells, serving as a positive control. Cells were washed 3 times in PBS (pH 7.3-7.5, #28374, Thermo Fisher). Cells were incubated in DMEM (300 µl; #31053028, Thermo Fisher) and 3-(4,5-dimethylthiazol-2-yl)-2,5-diphenyl tetrazolium bromide (MTT, 0.5mg/ml, #V13154, Thermo Fisher) for 1 h. Media was aspirated, and cells were incubated in dimethyl sulfoxide (300 µl; DMSO, #D8418, Millipore Sigma) for 10 minutes in the dark. DMSO was transferred into a clear 96-well plate (#82050, VWR, Radnor, PA) and absorbance was measured at 580 nm using a plate reader (SpectraMax iD3, Molecular Devices, San Jose, CA).

References

1. Scales, C. D., Smith, A. C., Hanley, J. M. & Saigal, C. S. Prevalence of Kidney Stones in the United States. *Eur. Urol.* **62**, 160–165 (2012).
2. Fontenelle, L. F. & Sarti, T. D. Kidney Stones: Treatment and Prevention. *Am. Fam. Physician* **99**, 490–496 (2019).
3. Pearle, M. S., Calhoun, E. A., Curhan, G. C. & null, null. Urologic diseases in america project: urolithiasis. *J. Urol.* **173**, 848–857 (2005).
4. Hyams, E. S. & Matlaga, B. R. Economic impact of urinary stones. *Transl. Androl. Urol.* **3**, 27883–27283 (2014).
5. Wu, C.-F., Shee, J.-J., Lin, W.-Y., Lin, C.-L. & Chen, C.-S. Comparison between extracorporeal shock wave lithotripsy and semirigid ureterorenoscope with holmium: YAG laser lithotripsy for treating large proximal ureteral stones. *J. Urol.* **172**, 1899–1902 (2004).
6. Parker, B. D., Frederick, R. W., Reilly, T. P., Lowry, P. S. & Bird, E. T. Efficiency and cost of treating proximal ureteral stones: Shock wave lithotripsy versus ureteroscopy plus holmium:yttrium-aluminum-garnet laser. *Urology* **64**, 1102–1106 (2004).
7. Erhard, M., Salwen, J. & Bagley, D. H. Ureteroscopic Removal of Mid and Proximal Ureteral Calculi. *J. Urol.* **155**, 38–42 (1996).
8. Fuchs, G. J. Ultrasonic lithotripsy in the ureter. *Urol. Clin. North Am.* **15**, 347–359 (1988).
9. Denstedt, J. D. & Clayman, R. V. Electrohydraulic Lithotripsy of Renal and Ureteral Calculi. *J. Urol.* **143**, 13–17 (1990).
10. Sözen, S. *et al.* Management of Ureteral Stones with Pneumatic Lithotripsy: Report of 500 Patients. *J. Endourol.* **17**, 721–724 (2003).
11. Jr, K., Pillai, Smith, Chrisofos, & Tolley. Electrokinetic lithotripsy: safety, efficacy and limitations of a new form of ballistic lithotripsy. *BJU Int.* **84**, 261–263 (1999).
12. Dretler, S. P. Laser lithotripsy: A review of 20 years of research and clinical applications. *Lasers Surg. Med.* **8**, 341–356 (1988).
13. Johnson, D. E., Cromeens, D. M. & Price, R. E. Use of the holmium:YAG laser in urology. *Lasers Surg. Med.* **12**, 353–363 (1992).
14. Helfmann, J. & Müller, G. Laser Lithotripsy: Process and Overview. *Med. Laser Appl.* **16**, 30–37 (2001).
15. Fried, N. M. Recent advances in infrared laser lithotripsy. *Biomed. Opt. Express* **9**, 4552–4568 (2018).
16. Yiu, M. k., Liu, P. l., Yiu, T. f. & Chan, A. y. t. Clinical experience with holmium:YAG laser lithotripsy of ureteral calculi. *Lasers Surg. Med.* **19**, 103–106 (1996).

17. Sandhu, A. *et al.* Holmium : YAG Laser for Intra Corporeal Lithotripsy. *Med. J. Armed Forces India* **63**, 48–51 (2007).
18. Marguet, C. G. *et al.* In vitro comparison of stone retropulsion and fragmentation of the frequency doubled, double pulse nd:yag laser and the holmium:yag laser. *J. Urol.* **173**, 1797–1800 (2005).
19. Raza, A., Turna, B., Smith, G., Moussa, S. & Tolley, D. A. Pediatric urolithiasis: 15 years of local experience with minimally invasive endourological management of pediatric calculi. *J. Urol.* **174**, 682–685 (2005).
20. Reddy, P. P. *et al.* Initial experience with endoscopic holmium laser lithotripsy for pediatric urolithiasis. *J. Urol.* **162**, 1714–1716 (1999).
21. Wollin, T. A. *et al.* Holmium: yag lithotripsy in children. *J. Urol.* **162**, 1717–1720 (1999).
22. Watterson, J. D. *et al.* Ureteroscopy and holmium:YAG laser lithotripsy: an emerging definitive management strategy for symptomatic ureteral calculi in pregnancy. *Urology* **60**, 383–387 (2002).
23. Watterson, J. D. *et al.* Safety and Efficacy of Holmium: Yag Laser Lithotripsy in Patients With Bleeding Diatheses. *J. Urol.* **168**, 442–445 (2002).
24. Gupta, P. K. Is the Holmium:YAG Laser the Best Intracorporeal Lithotripter for the Ureter? A 3-year Retrospective Study. *J. Endourol.* **21**, 305–309 (2007).
25. Türk, C. *et al.* EAU Guidelines on Interventional Treatment for Urolithiasis. *Eur. Urol.* **69**, 475–482 (2016).
26. Kronenberg, P. & Traxer, O. In vitro fragmentation efficiency of holmium: yttrium-aluminum-garnet (YAG) laser lithotripsy – a comprehensive study encompassing different frequencies, pulse energies, total power levels and laser fibre diameters. *BJU Int.* **114**, 261–267 (2014).
27. Bader, M. J. *et al.* Impact of pulse duration on Ho:YAG laser lithotripsy: fragmentation and dusting performance. *World J. Urol.* **33**, 471–477 (2015).
28. Elhilali, M. M., Badaan, S., Ibrahim, A. & Andonian, S. Use of the Moses Technology to Improve Holmium Laser Lithotripsy Outcomes: A Preclinical Study. *J. Endourol.* **31**, 598–604 (2017).
29. Kronenberg, P. & Somani, B. Advances in Lasers for the Treatment of Stones—a Systematic Review. *Curr. Urol. Rep.* **19**, 45 (2018).
30. Black, K. M. *et al.* Pulse modulation with Moses technology improves popcorn laser lithotripsy. *World J. Urol.* **39**, 1699–1705 (2021).
31. Giglio, N. C., Hutchens, T. C., South, A. A. & Fried, N. M. Dynamic properties of surfactant-enhanced laser-induced vapor bubbles for lithotripsy applications. *J. Biomed. Opt.* **26**, 018001 (2021).
32. Saeed, W. M., Hutchens, T. C. & Fried, N. M. Comparison of two surfactants for enhancing laser-induced vapor bubble dimensions. in *Advanced Photonics in Urology 2023* vol. 12353 8–12 (SPIE, 2023).
33. Blackmon, R. L., Fried, N. M. & Irby, P. B. Comparison of holmium:YAG and thulium fiber laser lithotripsy: ablation thresholds, ablation rates, and retropulsion effects. *J. Biomed. Opt.* **16**, 071403 (2011).
34. Dymov, A. *et al.* V11-11 thulium lithotripsy: from experiment to clinical practice. *J. Urol.* **197**, e1285–e1285 (2017).
35. Fan, X. *et al.* PEDOT:PSS for Flexible and Stretchable Electronics: Modifications, Strategies, and Applications. *Adv. Sci.* **6**, 1900813 (2019).
36. He, H. & Ouyang, J. Enhancements in the Mechanical Stretchability and Thermoelectric Properties of PEDOT:PSS for Flexible Electronics Applications. *Acc. Mater. Res.* **1**, 146–157 (2020).
37. Yang, Y., Deng, H. & Fu, Q. Recent progress on PEDOT:PSS based polymer blends and composites for flexible electronics and thermoelectric devices. *Mater. Chem. Front.* **4**, 3130–3152 (2020).
38. Hu, Z., Zhang, J., Hao, Z. & Zhao, Y. Influence of doped PEDOT:PSS on the performance of polymer solar cells. *Sol. Energy Mater. Sol. Cells* **95**, 2763–2767 (2011).
39. Hu, L., Song, J., Yin, X., Su, Z. & Li, Z. Research Progress on Polymer Solar Cells Based on PEDOT:PSS Electrodes. *Polymers* **12**, 145 (2020).

40. Li, J., Li, Z., Wang, J. & Chen, X. Study of conductive polymer PEDOT: PSS for infrared thermal detection. *Opt. Mater. Express* **9**, 4474–4482 (2019).
41. Zhang, X., Yang, W., Zhang, H., Xie, M. & Duan, X. PEDOT:PSS: From conductive polymers to sensors. *Nanotechnol. Precis. Eng.* **4**, 045004 (2021).
42. Muro, K., Watanabe, M., Tamai, T., Yazawa, K. & Matsukawa, K. PEDOT/PSS nanoparticles: synthesis and properties. *RSC Adv.* **6**, 87147–87152 (2016).
43. Zozoulenko, I. *et al.* Polarons, Bipolarons, And Absorption Spectroscopy of PEDOT. *ACS Appl. Polym. Mater.* **1**, 83–94 (2019).
44. Ho, D. S. *et al.* The Role of Cavitation in Energy Delivery and Stone Damage During Laser Lithotripsy. *J. Endourol.* **35**, 860–870 (2021).
45. Chen, J. *et al.* Cavitation Plays a Vital Role in Stone Dusting During Short Pulse Holmium:YAG Laser Lithotripsy. *J. Endourol.* **36**, 674–683 (2022).
46. Majaron, B., Plestenjak, P. & Lukač, M. Thermo-mechanical laser ablation of soft biological tissue: modeling the micro-explosions. *Appl. Phys. B* **69**, 71–80 (1999).
47. Aldoukhi, A. H., Ghani, K. R., Hall, T. L. & Roberts, W. W. Thermal Response to High-Power Holmium Laser Lithotripsy. *J. Endourol.* **31**, 1308–1312 (2017).
48. Hein, S., Petzold, R., Schoenthaler, M., Wetterauer, U. & Miernik, A. Thermal effects of Ho: YAG laser lithotripsy: real-time evaluation in an in vitro model. *World J. Urol.* **36**, 1469–1475 (2018).